



Technical Note

# A Year of Volcanic Hot-Spot Detection over Mediterranean Europe Using SEVIRI/MSG

Catarina Alonso <sup>1,2</sup>, Rita Durão <sup>1,3</sup> and Célia M. Gouveia <sup>1,4,\*</sup>

<sup>1</sup> Instituto Português do Mar e da Atmosfera, I.P., Rua C do Aeroporto, 1749-077 Lisboa, Portugal; catarina.alonso@ipma.pt (C.A.)

<sup>2</sup> Centre for the Research and Technology of Agroenvironmental and Biological Sciences (CITAB), Universidade de Trás-os-Montes e Alto Douro, 5000-801 Vila Real, Portugal

<sup>3</sup> Instituto Dom Luiz, Faculdade de Ciências, Universidade de Lisboa, 1749-016 Lisboa, Portugal

<sup>4</sup> Centro de Recursos Naturais e Ambiente, Instituto Superior Técnico, Universidade de Lisboa, 1049-001 Lisboa, Portugal

\* Correspondence: celia.gouveia@ipma.pt; Tel.: +351-21-844-70-00

**Abstract:** Volcano eruption identification and watching is crucial to better understanding volcano dynamics, namely the near real-time identification of the eruption start, end, and duration. Eruption watching allows hazard assessment, eruption forecasting and warnings, and also risk mitigation during periods of unrest, to enhance public safety and reduce losses from volcanic events. The near real-time fire radiative power (FRP) product retrieved using information from the SEVIRI sensor onboard the Meteosat Second Generation (MSG) satellite are used to identify and follow up volcanic activity at the pan-European level, namely the Mount Etna and Cumbre Vieja eruptions which occurred during 2021. The FRP product is designed to record information on the location, timing, and fire radiative power output of wildfires. Measuring FRP from SEVIRI/MSG and integrating it over the lifetime of a fire provides an estimate of the total Fire Radiative Energy (FRE) released. Together with FRP data analysis, SO<sub>2</sub> data from the Copernicus Atmosphere Monitoring Service (CAMS) is used to assess the relationship between daily emitted concentrations of SO<sub>2</sub> and the radiative energy released during volcanic eruptions. Results show that the FRE data allows us to evaluate the amount of energy released and is related to the pollutant concentrations from volcanic emissions during the considered events. A good agreement between FRP detection and SO<sub>2</sub> atmospheric concentrations was found for the considered eruption occurrences. The adopted methodology, due to its simplicity and near real-time availability, shows potential to be used as a management tool to help authorities monitor and manage resources during ongoing volcanic events.

**Keywords:** fire radiative power; SO<sub>2</sub> concentrations; CAMS; Mount Etna; Cumbre Vieja



**Citation:** Alonso, C.; Durão, R.; Gouveia, C.M. A Year of Volcanic Hot-Spot Detection over Mediterranean Europe Using SEVIRI/MSG. *Remote Sens.* **2023**, *15*, 5219. <https://doi.org/10.3390/rs15215219>

Academic Editors: Jon Atli Benediktsson, Bo-Hui Tang and Giuliana Bilotta

Received: 14 July 2023

Revised: 23 October 2023

Accepted: 26 October 2023

Published: 3 November 2023



**Copyright:** © 2023 by the authors. Licensee MDPI, Basel, Switzerland. This article is an open access article distributed under the terms and conditions of the Creative Commons Attribution (CC BY) license (<https://creativecommons.org/licenses/by/4.0/>).

## 1. Introduction

During the last 3 decades of the 20th century, according to the Global Assessment Report on Disaster Risk Reduction 2022 [1], around 90 to 100 medium- and large-scale disasters were reported per year. The large-scale disasters, such as earthquakes, tsunamis, volcanic eruptions, typhoons, and also extreme climate events, such as droughts, occur and adversely affect societies worldwide, requiring national and international assistance. Between 2001 and 2020, the number of these events increased from 350 to 500 per year [1].

Volcanic activity influences the atmosphere and climate on a hemispheric and global scale. The Hekla and Laki eruptions in June 1783 in Iceland and the Tambora eruption in April 1815 have been associated with their following cold winter and springs, which consequently were responsible for crop losses, widespread famine, and diseases over Europe [2–5]. The Etna eruptions between the 18th and 19th centuries were also followed by crop losses [6]. At present, volcanic activity in Europe still has strongly adverse socio-economic impacts in Europe and worldwide. An example is the Eyjafjallajökull eruption

(Iceland) in 2010, which, despite being a moderate-scale volcanic eruption, had plumes of volcanic ash that were transported on northwesterly winds towards continental Europe, causing the closure of European airspace and costing USD 5 billion to the global economy [4,7,8]. Although not associated with crop losses and famine, the volcanic eruption of La Palma in 2021 increased the levels of several elements associated with the deposition of ash and nanoparticles of magmatic material on the surface of bananas during their growing on farms in the affected area. However, the concentration of these elements vanished with washing in the processing plants and did not exceed 5% of the daily intake tolerance [9].

In line with the Sendai Framework Terminology on Disaster Risk Reduction 2015–2030, disaster risk reduction strategies and policies should be implemented, namely the creation of effective end-to-end and people centered early warning systems that may include, among other key elements, the detection, monitoring, and forecasting of the hazards and possible consequences. Nonetheless, some high-exposure volcanoes remain unmonitored, and more than 800 million people live within 100 km of a volcano that could erupt [10].

The monitoring of volcanic activity provides relevant information to better understand the structure and dynamics of volcanoes, and is crucial for hazard assessment, eruption forecasting, and warnings, as well as for risk mitigation during volcanic unrest [11]. However, monitoring volcanic activity is a complex matter that includes specific actions to constantly and in real-time acquire parameters that describe the state of a volcano [12–17]. During volcanic eruptions, significant amounts of ash particles and gases are injected into the atmosphere, interacting with anthropogenic activities and ecosystems on various levels [18,19]. Lava flows can also cause massive destruction and devastation, overwhelming whole villages, burying key infrastructure, and rendering land unproductive or uninhabitable [20]. Volcanic eruptions and volcanic earthquakes are also frequently associated with ground deformation during eruptive events [21]. Depending on the eruption characteristics, ejected materials can reach the troposphere or stratosphere, affecting the global radiative balance and surface temperatures [18,22]. Despite this important role as a natural force of the climatic system, volcanic activity also impacts air quality (generating low levels of air quality) and airspace security (e.g., by reducing visibility and potentially damaging aircraft engines) [23]. Therefore, following up on volcanic activity and monitoring volcanic materials (ash and gases) is revealed to be of primary importance, since it is the only way to avoid and mitigate their harmful effects [1,10].

Regarding the several volcanic materials released into the atmosphere, SO<sub>2</sub> is the most common gas, with its ejected amounts directly linked to the volcano's eruption explosivity [19,23]. Generally, SO<sub>2</sub> concentrations are slowly removed from the emitted plumes, having an important impact on the climate through radiative forcing, which could produce either surface cooling or surface warming effects at local and/or global scales [23–26]. In the troposphere, sulfur compounds accelerate the oxidation of metals, and volcanic sulfate aerosol has been implicated in some aviation incidents [27]. Volcanic sulfate aerosol can remain in the stratosphere for months and even years, depending on the SO<sub>2</sub> ejection altitude, total mass loading, latitudes, and dispersion patterns [28,29]. Moreover, SO<sub>2</sub> exposure may cause negative effects on health and the environment [30–32]. Namely, short-term exposures to this gas can irritate the eyes, harm the human respiratory system, and make breathing difficult. People with asthma, particularly children, are the most sensitive to these effects due to airway constriction [31]. SO<sub>2</sub> exposure has also been linked to cardiovascular diseases [31]. Additionally, high concentrations of SO<sub>2</sub> have harmful effects on trees and plants, by damaging foliage and decreasing growth. Furthermore, it can contribute to acid rain which can harm sensitive ecosystems, and by reacting with other compounds in the atmosphere to form fine particles, it may also reduce visibility (haze) over affected areas [31,32].

The use of remote sensing data is a useful approach to conveniently assess volcanic activity, allowing early and rapid detection, quantitative characterization, plume tracking, eruption forecasting, and specifically allowing for the monitoring of remote inaccessible

volcanic areas at different time scales [19,23,33]. Particularly, the evolution of satellites in recent years has marked a great advance in the proximal and distal monitoring of volcanic eruptions in areas with scarce instrumentation and/or difficult access [18,34]. Geostationary satellites offer a unique opportunity to follow up, in near real-time, the entire evolution of volcanic eruptions, such as Mount Etna [35,36], expanding monitoring capabilities on an hourly basis, with a time step of 10 or 15 min [18,24,37]. By monitoring a volcanic eruption in near real-time, geostationary satellites can help to reduce risks to the population and local air traffic, as well as to detect different types of volcanic activity [19,33]. Additionally, sensing-based tools are less cost-effective when compared to ground-based monitoring instrumentation, which is more vulnerable to destruction by volcanic activity, theft, or burns [34].

The Fire Radiate Power (FRP) product, derived from the Spinning Enhanced Visible and InfraRed Imager (SEVIRI) instruments on board the Meteosat Second Generation (MSG) geostationary satellite, has been delivered in near real-time since 2004. The FRP was originally designed to record information on the location, timing, and radiative power emitted by wildfires (in MWatts), detected every 15 min across the full MSG disk, at the native spatial resolution of the SEVIRI sensor (3 km at the sub-satellite point). Therefore, FRP quantifies the release rate of radiant energy by a fire, over all wavelengths, based on Stefan's Law, which relates total emitted radiance over all wavelengths (i.e., the Fire Radiative Power) to emitter temperature [38]. Likewise, the thermal emission of an active volcanic surface relates directly to the radiative power of the emitter at a specific time. By definition, the FRP algorithm assumes that the fire temperature ranges from 665 K to 1365 K [38]; on the other hand, lava and magma temperatures range from 1073 K to 1473 K [39]. For example, in fire case studies, FRP is used as a proxy for fireline intensity, helping to develop mitigation strategies [40,41], whereas in the case of volcanic events, it is expected that it can be used to understand eruption dynamics and the direction of lava flow, to assess dangerous areas and issue evacuation alerts.

In recent years, Mount Etna in Italy has been permanently active. However, in 2021, strong eruptive activity was reported over Mount Etna, and also over the Cumbre Vieja in the Canary Islands, which has not been volcanically active since 1971 [6,42–47]. In the present work, geostationary data are used to show the satellite's ability to identify in near real-time the effusive volcanic eruptions that occurred during 2021 in Mediterranean Europe, identifying the start and the end of the eruptions, and demonstrating how to keep watching for volcanic activity by assessing the energy and the SO<sub>2</sub> released during the effusive volcanic events. In order to early detect the hotspots and to assess the intensity of the Mount Etna and Cumbre Vieja eruptions, the near real-time FRP was retrieved from the product, using information from SEVIRI sensor onboard of MSG satellite. Since the radiative power emitted by fires can be related to the production of smoke during combustion [38], the potential of using FRP also as a proxy for volcanic gas emissions, namely SO<sub>2</sub>, is also evaluated in this work. Hence, the concentration of the SO<sub>2</sub> released in areas surrounding the volcano was characterized for each event, to assess the respective spatio-temporal patterns, based on data provided by the Copernicus Atmosphere Monitoring Service (CAMS). Consequently, by assessing the relationship between daily emitted SO<sub>2</sub> concentrations and the radiative energy released during volcanic eruptions, it is also possible to assess the exposure to SO<sub>2</sub> concentrations from active volcanoes, with respect to the air quality guideline values for the general population and ecosystems.

## 2. Data and Methods

### 2.1. Study Area

Mount Etna is a basaltic volcano located on the eastern coast of Sicily, Italy, and has had eruptions that date back 3500 years [6,48,49]. It is one of the most active volcanoes in the world [6], representing a potential hazard for about 600,000 people living on its slopes, as well as hundreds of thousands of tourists who visit the volcano yearly [32], due to the possibility of flank eruptions like the 1669 eruptions [50,51]. The volcanic activity of Mount

Etna, which can be both explosive and effusive, has been particularly active and intense in the last 30 years [20,42–45].

The Cumbre Vieja is historically the most active volcano in the Canary Islands, in Spain. After 50 years of sleeping, the Cumbre Vieja volcano woke up with an eruptive episode on 19 September that lasted until 13 December 2021 [46]. For three months, the Cumbre Vieja eruption produced lava fountains and lava flows and injected ash and gases into the atmosphere. The appearance of this eruptive event forced the evacuation of about 6400 residents and destroyed infrastructure worth more than EUR 400 million [46].

The methodology used to identify and follow-up volcanic hotspots on European islands during 2021's eruptive events was performed over the following volcanic surrounding areas: [14.4E–15.6E; 37.4N–38.2N] for Mount Etna, and [18.2W–17.4W; 28.4N–28.8N] for Cumbre Vieja. These areas correspond to the areas inside the dashed boxes in Figure 1.

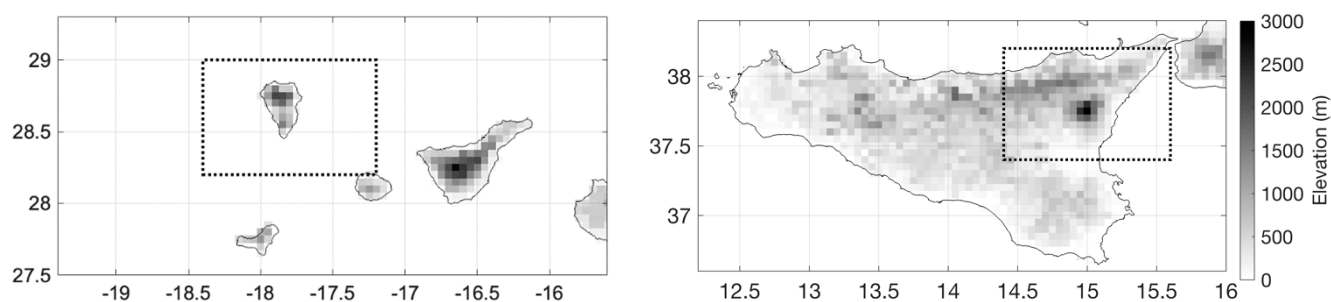


**Figure 1.** Study area inside the dashed box: Mount Etna (right panel) and the Cumbre Vieja (left panel). Elevation map is represented by gray colors (unit: meters).

## 2.2. Data

The FRP is derived from the SEVIRI instruments on board the MSG geostationary satellite, delivered in near real-time, since 2004, by the EUMETSAT Land Surface Analysis Satellite Applications Facility (LSA-SAF).

The FRP product (LSA-502) is spread across the full spatiotemporal resolution of the SEVIRI imager, with a 3 km spatial sampling distance at the sub-satellite point (decreasing away from the West African sub-satellite point) and with a temporal resolution of 15 min. The FRP of a pixel exhibiting a strong thermal contrast with its neighborhood and with a power typical of fire activity, an active fire pixel, is expressed in megawatts (MW) and represents the amount of radiant heat energy emitted, per time unit, by the burning vegetation and/or organic soils present within that pixel. The FRP algorithm confidently detects active fire pixels whose FRP exceeds 30 MW [38] and can discriminate the area of actively burning fires, covering down to  $10^{-4}$  of a pixel, being, therefore, more sensitive to fire than other algorithms that are used in many active fire products, which are widely exploited [38]. A full description of the FRP/MSG operational algorithm is detailed by Wooster et al. (2015) [38].

In the normal state of persistent activity of Mount Etna, mild explosive activity is usually concentrated at the summit craters, where the lava extrudes at a nearly constant temperature of around 1350 K, and during stronger paroxysmal eruptions the lava temperature is higher (~1400 K) [35,36,52]. Conversely, for the Cumbre Vieja eruption in 2021, it is estimated that the lava temperatures ranged approximately from 1373 K to 1433 K [53–56]. As these temperature values are included in the temperature spectrum detected by the FRP algorithm, it follows that this product can be properly used to detect the radiative power characteristic of volcanoes.

The SO<sub>2</sub> concentrations were obtained through the global atmospheric composition forecasts (GACF) data from Copernicus Atmosphere Monitoring Service (CAMS), a component of the European Earth Observation program, Copernicus. GACF are produced twice a day, on more than 50 chemical species and seven different types of aerosols. For each forecast, the initial conditions are obtained by combining a previous forecast with

current satellite observations of aerosol optical depth, ozone (O<sub>3</sub>), carbon monoxide (CO), nitrogen dioxide (NO<sub>2</sub>), and sulfur dioxide (SO<sub>2</sub>) through the 4D-VAR data assimilation process, providing a complete and consistent dataset that enables estimations at sites where observation coverage is poor or for atmospheric pollutants for which no direct observations are available (<https://ads.atmosphere.copernicus.eu>, accessed on 31 March 2022). GACF are available on a regular 0.44° × 0.44° resolution grid (~48 km), from 2015 up to now, at hourly resolution.

For the present study, SO<sub>2</sub> data, namely the total column sulfur dioxide, was selected at the surface level, and was used to assess the spatial and temporal patterns of concentrations emitted into the atmosphere during the Mount Etna and Cumbre Vieja eruptions in 2021, over the defined study areas above.

### 2.3. Methods

In this work, the FRP was used to identify and analyze the periods of the highest activity on Mount Etna and Cumbre Vieja, in terms of emitted radiative energy, and the start and the end date of the eruption.

Integrating the FRP obtained from SEVIRI/MSG with the temporal resolution of 15 min over the lifetime of fire makes it possible to estimate the total Fire Radiative Energy (FRE) released during the event. The adopted methodology relies on the fact that released FRE is proportional to the amount of biomass consumed and therefore to the intensity of the eruption, computed using the accumulated FRP of each event [57,58]. The hourly and daily FRE was calculated for each volcanic event using the formula by Pinto et al. 2018 [58]. The hourly energy emitted by the volcano at a specific pixel was computed by integrating the radiative power measured via SEVIRI in that pixel over the considered hour. Since the data are collected every 15 min, the hourly energy, FRE (in gigajoules, GJ), for each pixel  $p$  and hour  $h$  could be estimated using the following Equation (1):

$$FRE_{ph} = 0.9 * \left( \sum_{k=1}^4 FRP_p \right)_{hr} \quad (1)$$

where the index  $k$  indicates the sequence of 15 min of each hour,  $FRP_p$  is the fire radiative power (in MW) in pixel  $p$ , and the 0.9 is a factor that converts the result into GJ. Subsequently, the daily  $FRE_{pd}$  is the accumulated hourly  $FRE_{ph}$ , over the 24 h  $h$ , for each pixel  $p$ . The hourly and daily FRE for the study areas correspond to the hourly and daily accumulated FRE of all pixels present in the study areas.

The daily released SO<sub>2</sub> concentration was obtained by the accumulated value of all GACF pixels in the surrounding areas of the volcano, previously defined above. Maps of daily SO<sub>2</sub> concentrations for the period of the eruptive events were also produced for the two studied areas of Figure 1. To analyze the temporal evolution of FRE and SO<sub>2</sub> emissions related to the volcano's eruptions, the hourly and daily accumulated values of FRE and SO<sub>2</sub> concentration were summed over the boxes defined inside Figure 1.

In order to evaluate the agreement between FRE and SO<sub>2</sub> emissions, two eruptive periods with similar length were selected, January to April in the case of Mount Etna, and September to December for the Cumbre Vieja. For each of them, the daily FRE and SO<sub>2</sub> values from the previously defined boxes were accumulated every 8 days.

## 3. Results

### 3.1. Volcanic Activity in Mount Etna

The periods of volcanic activity for Mount Etna, as obtained using the daily FRE accumulated for the selected box, and over the entire year of 2021, are shown in Figure 2. The higher daily values of FRE associated with the moments of greatest volcanic activity occurred during February, April, June, July, and August (Figure 2, upper panel). High activity spanning over several consecutive days is observed during February and July. The bottom panels of Figure 2 show the hourly periods of FRE during these two months, allowing us to identify the beginning of eruptive events and the moments of high explosive

activity. The maximum hourly FRE values observed during the analyzed months occurred on 4 March, at 9 a.m., reaching a radiative power of about 35 TJ, and the second maximum occurred on 4 July at 4 p.m., with an emitted radiative power of the same magnitude, exceeding 30 TJ (Figure 2, bottom panels). High emitted radiative power values are also observed for 12 and 31 March, and 2, 7, 8 and, 31 July (Figure 2, bottom panels).

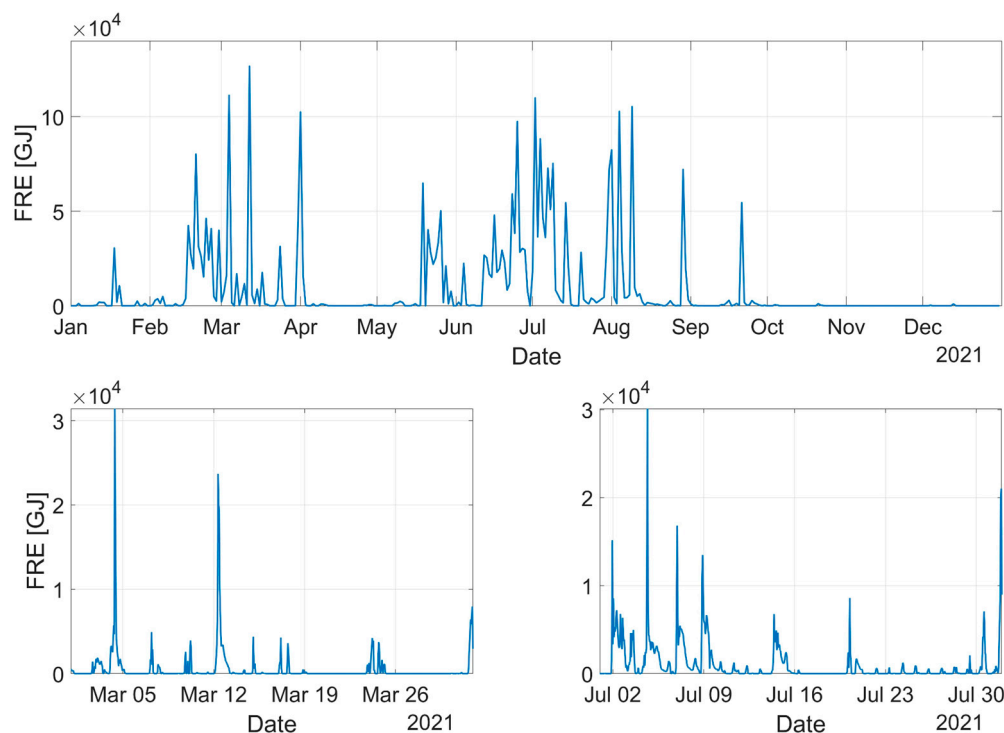


**Figure 2.** Daily FRE (GJ) accumulated over the dashed box for Mount Etna in Figure 1, covering the total period (top panel) and the hourly FRE (GJ) for March (left bottom panel) and July (right bottom panel).

The daily FRE accumulated over the selected box, considering the Etna Eruption in 2021, is observed in Figure 3 (blue line). The maximum of daily FRE released occurred on 12 March, with a release of 126 TJ. Other relative maxima are observed on 4 March (111 TJ), 1 April (102 TJ), and 9 August (105 TJ). It should be stressed that the FRE and FRE maximum values may not occur on the same day, because the maximum FRE corresponds to the day with the longest continuous and intense volcanic activity and not to the day of maximum FRE emission. However, for the period and area under analysis, 4 March was the second day with the highest FRE released, in agreement with the observed in Figure 2. However, Figure 3 shows persistent volcanic activity for several days in February, March, June, and July.

The ejection of  $\text{SO}_2$  into the atmosphere during the months of the Mount Etna eruption resulted in three distinct peaks of daily maximum  $\text{SO}_2$  concentrations, as shown in Figure 3 (orange line). Namely, on 28 February, 1 April, and 16 June, with maximum released concentrations of  $1775 \mu\text{g}/\text{m}^3$ ,  $1823 \mu\text{g}/\text{m}^3$ , and  $1820 \mu\text{g}/\text{m}^3$ , respectively (Figure 3, line orange). It should be also noted that, as expected, daily concentrations of  $\text{SO}_2$  follow the intensity of the volcanic activity, revealing a similar temporal pattern as the FRE released during the Mount Etna eruption. This behavior pattern is evident on days with higher FRE values, such as 4 and 12 March (111 and 126 TJ), 1 April (102 TJ), and 9 August (105 TJ), where the concentration of  $\text{SO}_2$  is higher than  $1150 \mu\text{g}/\text{m}^3$  (Figure 3, blue line).

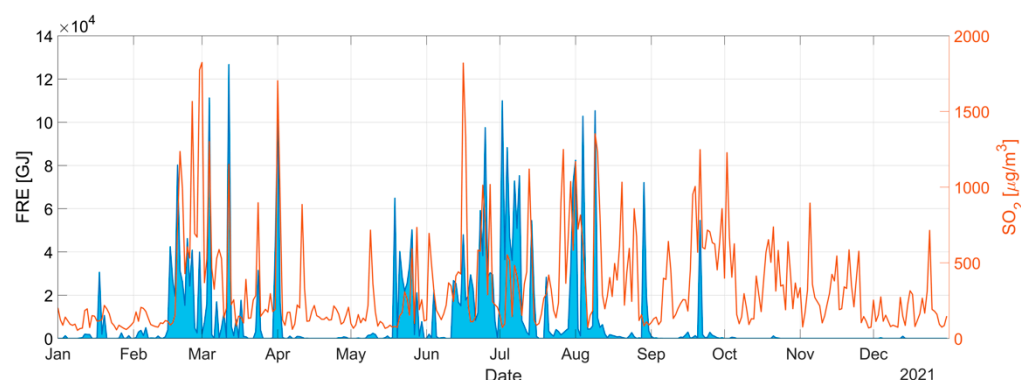


**Figure 3.** Daily FRE (blue, GJ) and  $\text{SO}_2$  (orange,  $\mu\text{g}/\text{m}^3$  accumulated over the dashed box for Mount Etna in Figure 1).

In order to better evaluate the impacts of  $\text{SO}_2$  emissions over the volcanic-affected areas, FRE and  $\text{SO}_2$  values were spatially represented, as can be seen in Figure 4, for two days of Etna's maximum volcanic activity, 4 March and 1 April. The daily concentrations of  $\text{SO}_2$  on 1 April were higher than on 4 March, however, on both days  $\text{SO}_2$  values were above  $300 \mu\text{g}/\text{m}^3$  over the volcano area. It also should be noted that the higher  $\text{SO}_2$  concentrations are located in the southeast part of the island, probably related to the movement of the plume to the south, associated with the prevalent wind direction of the considered days.

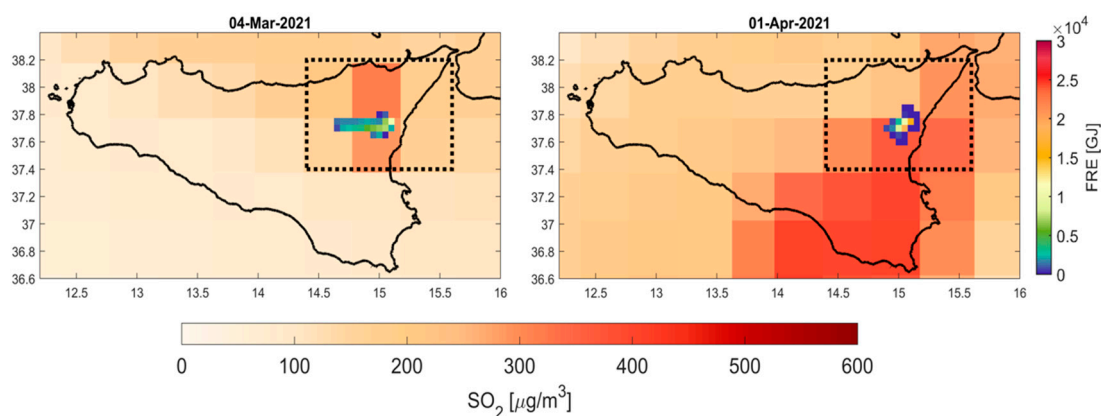


**Figure 4.** FRE (GJ) and  $\text{SO}_2$  ( $\mu\text{g}/\text{m}^3$ ) concentrations on 4 March (**left panel**) and FRE and  $\text{SO}_2$  concentrations on 1 April (**right panel**). The dashed rectangle represents the area where the accumulated FRP, FRE, and  $\text{SO}_2$  previously represented were calculated for Mount Etna.

The area around Mount Etna affected by volcanic activity, with respect to the energy released, was larger on 4 March (Figure 4, left panel), showing lower FRE pixels in locations at a greater distance from the center of the volcano. Although FRE values are lower on 4 March (maximum 10.54 TJ) than on 1 April (maximum 18.45 TJ), the FRE accumulated in the study area on 4 March is slightly higher (111 TJ) than on 1 April (102 TJ), as on 4 March the lava flow covered a greater number of pixels [35].

### 3.2. Volcanic Activity in the Cumbre Vieja

The periods of volcanic activity for the Cumbre Vieja, as obtained using the daily FRE accumulated for the selected box and over the entire year of 2021, are shown in Figure 5. The Cumbre Vieja's effusive volcanic activity began on 19 September and continued until 13 December, presenting the maximum radiative energy of around 80 TJ on 2 October and relative maxima on 17 and 21 October above 40 TJ (Figure 5, top panel). The radiative power was low and intermittent between the beginning of November and the first half of December. Figure 5 (bottom panel) shows the period of greatest activity of the volcano,

from 28 September until 12 October, on an hourly basis. It should be noted that FRE values were above 4 TJ several times between 1 October at 6 p.m. and 3 October at 7 p.m., reaching the maximum value on 1 October at 9 p.m. In addition to that period, values also above 4 TJ occurred on 28 September at 7 p.m. and 11 p.m., and 6 October at 6 p.m.

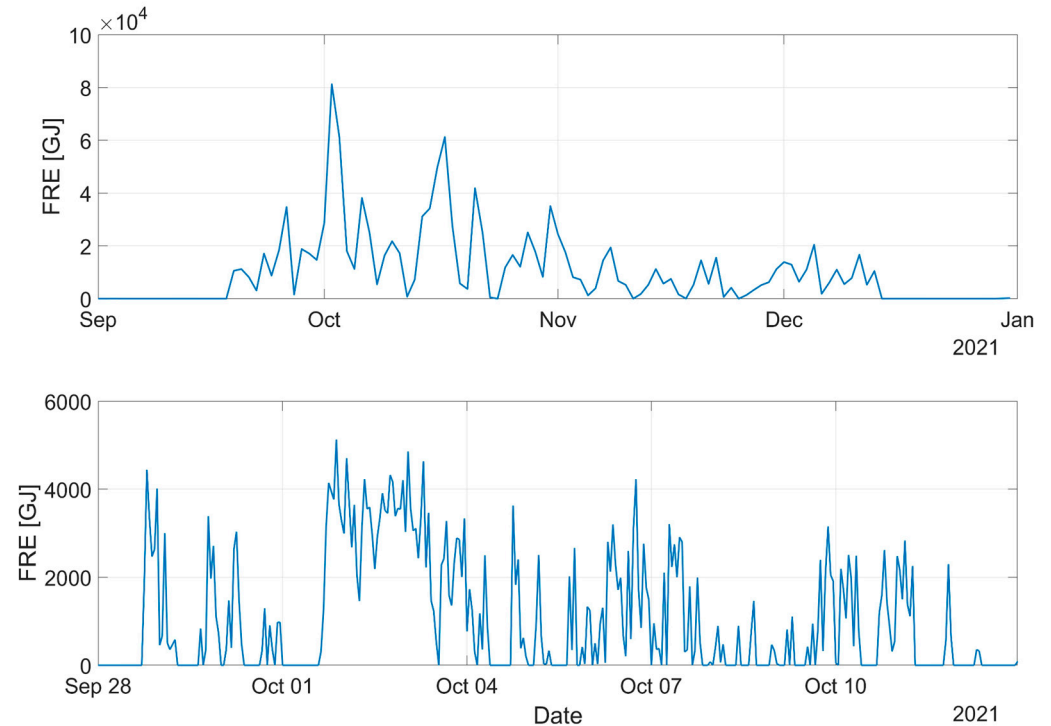


**Figure 5.** Daily FRE (GJ) from September to December (**top panel**) and hourly FRE (GJ) from 28 September to 12 October (**bottom panel**) for the Cumbre Vieja.

The daily FRE accumulated over the selected box, denoting the Cumbre Vieja, in 2021 is observed in Figure 6 (blue line). Intense volcanic activity, as derived from a daily accumulated radiative energy release of more than 7 TJ, is observed between 28 September and 28 October. It should be noted the FRE maximum value of around 8.1 TJ occurred on 2 October. A downward trend in FRE values is observed after the beginning of November, achieving negligible values of daily FRE in the second half of December (Figure 6, blue line).

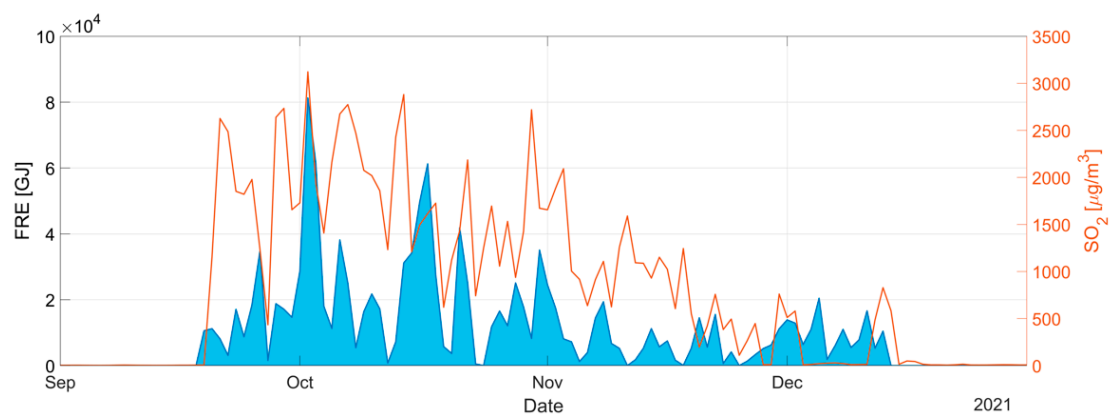


**Figure 6.** Daily FRE (blue, GJ) and SO<sub>2</sub> (orange,  $\mu\text{g}/\text{m}^3$ ) for the same area and period for the Cumbre Vieja.

The SO<sub>2</sub> concentrations released into the atmosphere during the Cumbre Vieja activity are also related to the FRE values emitted during the eruption periods, as expected. Both

the FRE maximum value (8.1 TJ) and SO<sub>2</sub> maximum concentration (3122 µg/m<sup>3</sup>) occurred on 2 October (Figure 6, orange line), and as the FRE diminished due to the volcano's activity decreasing, the SO<sub>2</sub> concentration also declined after 15 December.

Similarly to the Mount Etna event, two days with high FRE and SO<sub>2</sub> values were identified and spatially represented for the Cumbre Vieja eruption, 2 and 17 October, respectively (Figure 7). Regarding the FRE values at the pixel scale, on 17 October, the FRE values (2.7 TJ) were almost of the same magnitude as the FRE values released on the 2nd of October (FRE~2.5 TJ). However, on 2 October more active pixels were detected, making the daily accumulation in the volcano area higher than on 17 October. This behavior is also reinforced by the highest amounts of SO<sub>2</sub> released into the atmosphere on 2 October, above 500 µg/m<sup>3</sup>, whereas the concentration of SO<sub>2</sub> was below 300 µg/m<sup>3</sup> on 17 October.

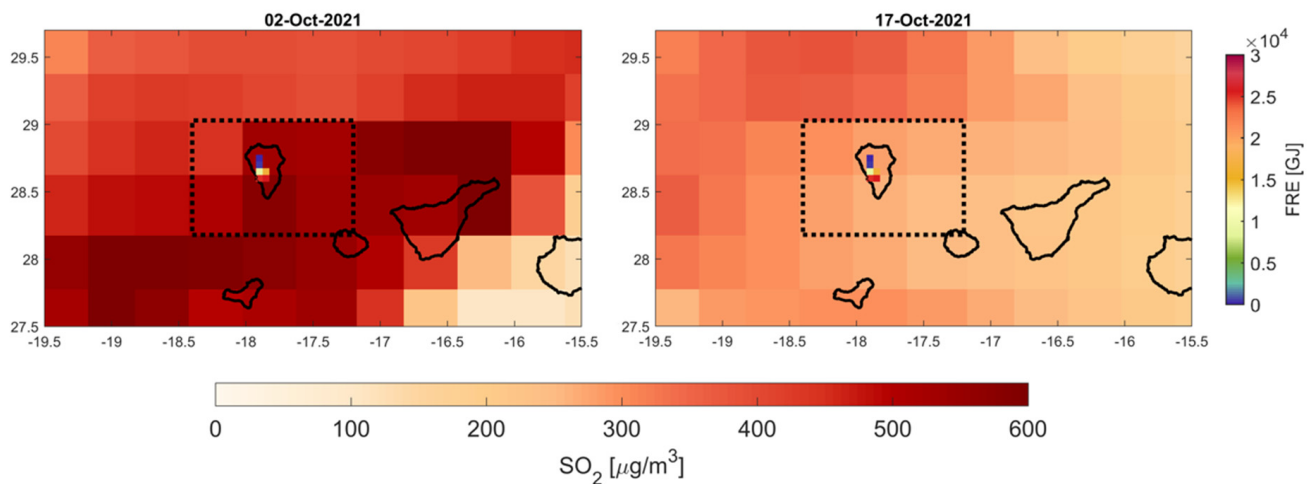


**Figure 7.** As in Figure 3, but for the Cumbre Vieja on (left panel) 2 October and on (right panel) 17 October 2021.

Mount Etna has hourly FRE values much higher than those reached by the Cumbre Vieja. When analyzing the two different eruption periods, January to April in the case of Mount Etna, and September to December for the Cumbre Vieja, there is a significant agreement between the FRE and SO<sub>2</sub> values accumulated every 8 days (Figure 8). Therefore, besides the FRE being an indicator of volcanic activity, it also agrees with the emitted SO<sub>2</sub> concentrations during both volcanic events. However, it should be stressed that it is not possible to compare the FRE from Etna and the Cumbre Vieja, as the number of pixels with FRE included in the considered box for Etna and Cumbre Vieja is different, but also mainly due to the different nature of the volcanic activity. On the other hand, the Cumbre Vieja activity was persistently high over a consecutive period of days showing continuously recorded high hourly FRE values. Since the FRE is the cumulative FRP, the maximum FRE reached by each volcanic eruption differs by a scale of only 4 GJ. Furthermore, Mount Etna has a larger area of volcanic activity pixels (Figure 4) than the Cumbre Vieja (Figure 7), which could also be a reason for the FRE value being higher for Mount Etna (Figure 3) than for the Cumbre Vieja (Figure 4). The different FRE patterns are certainly directly linked to the type of explosive volcanic eruption, which is also associated with the amounts of SO<sub>2</sub> released into the atmosphere, as previously shown. However, the analysis of the type of each volcanic eruption is beyond the scope of the present work.

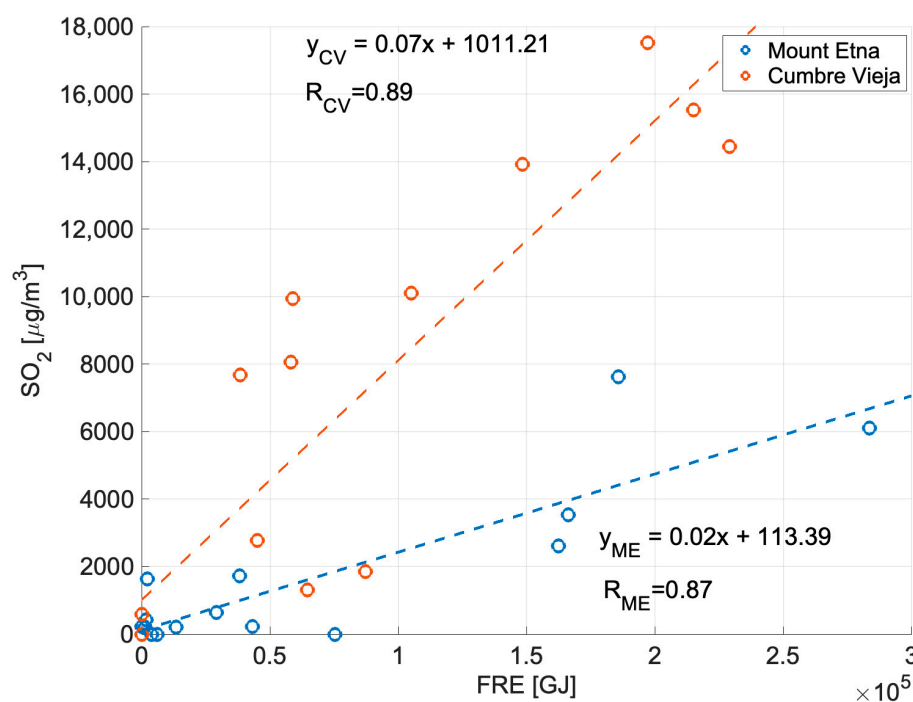


**Figure 8.** Scatter plot of FRE greater than 1 GJ and SO<sub>2</sub> greater than 200 µg/m<sup>3</sup>, values accumulated over 8 days between January and April for Mount Etna event (blue), and September and December for the Cumbre Vieja event (orange).

#### 4. Discussion

Volcanic eruptions are important natural sources of atmospheric pollutants due to the ejection of ash particles and gases—such as carbon dioxide (CO<sub>2</sub>), water vapor (H<sub>2</sub>O), and sulfur dioxide (SO<sub>2</sub>)—into the atmosphere [23]. Apart from the climate effects, volcano emissions also have important impacts on air quality and airspace security, making it necessary to monitor them [23], to better assess and anticipate their harmful impacts.

For example, Mount Etna’s mean SO<sub>2</sub> flux emitted was equivalent to the total of industrial France (~5000 T/day), making it the largest continuous point source of SO<sub>2</sub> globally [59]. On the other hand, when the Cumbre Vieja erupted on 19 September, the SO<sub>2</sub> plumes traveled mainly across Northern Africa and Southern Europe, probably affecting Northern and Western Europe [60]. After that, in early October, when the wind direction changed, the volcanic plumes were transported over long distances, reaching the Caribbean islands and decreasing local air quality levels, due to high SO<sub>2</sub> concentrations, together with the arrival of a Saharan dust intrusion [60].

According to reports issued by the Global Volcanism Program [61], the maximum FRE periods coincided with the days of high volcanic activity at the Mount Etna and Cumbre Vieja eruptions. Since December 2020, Mount Etna has had frequent strombolian explosions of variable intensity, effusive activity, ash emissions, and ashfall [35,61]. According to Ganci et al. (2023) [35], two main eruptive phases were identified, taking into account the lava volumes of the individual Etna events; which reveals a set of paroxysmal events separated by relative calm periods at Mount Etna [35,44,62]. Moreover, these eruptive phases are easily identified from the FRE patterns, presented in Figure 1, in agreement with the radiant heat flux curves and effusion rate estimates presented by the CL-HOTSAT thermal monitoring system [35]. Namely, the first eruptive phase lasted from 16 February to 1 April 2021, with the peak of paroxysmal activity on 4 March 2021, which is in agreement with the FRE patterns presented in Figures 1 and 3. For example, on 4 March, it was the 9th episode; at 8.50 a.m. there was strombolian activity with 300 m tall lava explosions, and ash plumes rose 11 km above the summit and caused lapilli to fall around the volcano (20 km). This episode agrees with the FRE and SO<sub>2</sub> values observed and presented in

Figures 3 and 4, respectively. On 31 March, there was a strong explosion followed by several clouds of ash, marking the beginning of the 17th episode of the lava fountains. Lava fountains continued to be visible during 1 April and intense strombolian activity produced dense plumes of ash that reached 9 km in altitude and drifted SSW, as is visible in Figure 3, left side. The INGV reported three episodes of lava fountaining from 28 June to 6 July [63]; the second episode began at 5 p.m. on 4 July, which was one of the maximum values of FRE identified (Figure 2).

In the Cumbre Vieja event, a fissure eruption began at 2 p.m. on 19 September, with a large explosion that produced a gas-and-ash plume at about 1 km in altitude [29]. The FRE may have detected the start of the eruption at 7 p.m. instead of 2 p.m. due to the plume of gas and ash preventing the satellite's sensors from accurately measuring the start of the eruption. Still, the maximum values of the FRE and SO<sub>2</sub> concentrations released from the Cumbre Vieja agree with the opening of two vents about 600 m NW of the main cone during late 30 September and 1 October, leading to strong volcanic activity on 2 October, with ash plumes rising to 3–5 km and drifting S [64], as can be seen in Figure 7- left panel.

The calculation of the accumulated value of the daily FRE, related to the time of each eruption, shows that the amount of energy released by volcanic activity is very high, in line with the eruption's intensity. Considering that 2000 GJ is the typical daily amount of energy released by a severe fire [58], the results reveal that these volcanic eruptions can release up to 40× to 60× more energy. However, it should be stressed that the FRP product is produced for cloud-free pixels and therefore the product seems to be inadequate for identifying and monitoring volcanic eruptions associated with big clouds of smoke, such as subplinian and plinian eruptions. Moreover, as the FRE is defined as the emitted radiant energy released during combustion, it can be linked to the fire's smoke production [65], and consequently, it can be used as a proxy for volcanic emissions into the atmosphere.

Furthermore, it can be concluded that FRP products allow for hazard assessment, early eruption forecasting, and warnings in near real-time at a global scale (including other geostationary satellites like HIMAWARY and GOES) in remote and isolated regions with a very low post-processing cost (only by computing FRE from FRP). However, a further detailed comparison with other thermal hotspot monitoring systems such as MODVOLC, MIROVA, or HOTVOLC, should be performed in order to better identify other regions and types of volcanic activity that could benefit from using the proposed tool. It also could be interesting to explore the use of the proposed approach to complete the CL-HOTSAT thermal monitoring system, using the FRP/FRE hotspots as early signs to identify severe eruptions, according to the magnitude of the emitted power or released energy.

Sulfur dioxide emissions affect the balance of the radiative forcing of climate, with several harmful consequences for human health activities and ecosystems. Thus, regarding the protection of human health and activities, there are two SO<sub>2</sub> limit values that should not be exceeded, according to the European Air Quality Directive (2008/EC/50) [66]: (i) the SO<sub>2</sub> hourly mean value may not exceed 350 µg/m<sup>3</sup> more than 24 times in a year, and (ii) the SO<sub>2</sub> daily mean value may not exceed 125 µg/m<sup>3</sup> more than 3 times in a year. Taking this into account, both SO<sub>2</sub> volcanic emissions considered here far exceeded the recommended human health thresholds. Namely, the Mount Etna eruption had 79 days with SO<sub>2</sub> concentrations over 500 µg/m<sup>3</sup>, whereas the Cumbre Vieja had 66 days with SO<sub>2</sub> concentrations higher than 500 µg/m<sup>3</sup>. With respect to what is known for each eruption, the Mount Etna and Cumbre Vieja volcanoes revealed different SO<sub>2</sub> plumes, due to the different eruptive activity and dynamics of each volcano and to different local/regional diffusion processes, which were also related to the local orography and meteorological influences. These released SO<sub>2</sub> concentrations are also in line with the observed FRE values, in accordance with the peaks of thermal radiance studied by Ganci et al. (2023) [35]; this corroborates the rationale that FRE can be used as a proxy for volcanic emissions into the atmosphere. Therefore, the proposed methodology, based on FRE data, shows that it is possible to assess potential exceedances of SO<sub>2</sub> threshold levels, allowing for the issuing

of several alerts to protect local populations from the adverse consequences of high SO<sub>2</sub> concentrations on human health and activities.

## 5. Conclusions

Identifying and monitoring volcanic activity on a real-time basis can help to reduce risks to the population and local air traffic, as well as obtain information about the processes and dynamics of volcanic eruptions. Moreover, it can contribute to avoiding their effects in the short-term (e.g., physical damage) and long-term (e.g., sustained or permanent displacement of populations).

The ground-based monitoring of volcanic activity, on a real-time basis, is a challenging task, as the instrumentation may be vulnerable to destruction or difficult to manage in remote locations. The present work explores the added value of using geostationary data to follow the entire evolution of volcanic eruptions, expanding monitoring capabilities on an hourly basis. The ability to monitor the area of a volcano every 15 min, using the FRP product from SEVIRI/MSG, allows for the identification of the moment of greatest volcanic activity, in near real-time. Despite the lower spatial resolution, the very high temporal resolution and low timeliness may represent a great advantage in comparison with polar satellite products that collect only two observations a day. It should be noted that this added value has been revealed to be higher at low to moderate latitudes where the accuracy of the FRP product is higher [38].

The adopted rationale relies on the fact that the FRE released is proportional to the intensity during the Mount Etna and Cumbre Vieja 2021 explosive volcanic eruptions, based on the accumulated radiative power released by each event [57,58]. Among the advantages of using the product are the high sensitivity that allows for detecting sub-pixel fires and the high temporal resolution (15 min) and the continuous watching of volcanic activity, making it possible to assess the rapid behavior and direction of the lava flow, almost in near real-time.

Considering that FRE is the emitted radiant energy released during combustion, linked to smoke production [40], the possibility of using it as a proxy for volcanic emissions into the atmosphere was also assessed. The very good results of the evaluation of the volcanic activity from the Mount Etna and Cumbre Vieja events show that FRP products can be a valuable proxy for volcanic activity. The released SO<sub>2</sub> concentrations during both eruptions are also in line with the emitted FRE values, corroborating the hypothesis that FRE can be used as a proxy for volcanic emissions into the atmosphere. Furthermore, the proposed methodology, due to its simplicity and near real-time availability, has potential to be used as a management tool to help authorities monitor and manage resources during ongoing volcanic events, contributing to risk mitigation during periods of unrest and reducing SO<sub>2</sub> exposure, enhancing public safety and reducing losses from volcanic events.

**Author Contributions:** Conceptualization, C.A., C.M.G. and R.D.; writing—original draft preparation, C.A.; review and editing, R.D.; visualization, C.A.; supervision, C.M.G. All authors have read and agreed to the published version of the manuscript.

**Funding:** This study was performed within the framework of the LSA-SAF, co-funded by EUMETSAT.

**Data Availability Statement:** Not applicable.

**Acknowledgments:** This study was performed within the framework of the project FAIR—Forecasting Air Quality in Portugal during wildfires and pollution outbreaks (reference 2022.01660.PTDC), funded by the FCT (Fundação para a Ciência e a Tecnologia, Portugal). We thank LSA-SAF and CAMS for providing FRP and SO<sub>2</sub> data. We are also indebted to four anonymous reviewers and the academic editor for their detailed comments and suggestions which helped to improve this paper.

**Conflicts of Interest:** The authors declare no conflict of interest.

## References

1. United Nations Office for Disaster Risk Reduction. *Global Assessment Report on Disaster Risk Reduction 2022: Our World at Risk: Transforming Governance for a Resilient Future*; UNDRR: Geneva, Switzerland, 2022; ISBN 92-1-001505-3.
2. Edwards, J.; Anchukaitis, K.J.; Gunnarson, B.E.; Pearson, C.; Seftigen, K.; von Arx, G.; Linderholm, H.W. The Origin of Tree-ring Reconstructed Summer Cooling in Northern Europe during the 18th Century Eruption of Laki. *Paleoceanogr. Paleoclimatology* **2022**, *37*, e2021PA004386. [[CrossRef](#)]
3. Trigo, R.M.; Vaquero, J.M.; Alcoforado, M.-J.; Barriendos, M.; Taborda, J.; García-Herrera, R.; Luterbacher, J. Iberia in 1816, the Year without a Summer. *Int. J. Climatol.* **2009**, *29*, 99–115. [[CrossRef](#)]
4. Mani, L.; Tzachor, A.; Cole, P. Global Catastrophic Risk from Lower Magnitude Volcanic Eruptions. *Nat. Commun.* **2021**, *12*, 4756. [[CrossRef](#)]
5. Wilson, N.; Valler, V.; Cassidy, M.; Boyd, M.; Mani, L.; Brönnimann, S. Impact of the Tambora Volcanic Eruption of 1815 on Islands and Relevance to Future Sunlight-Blocking Catastrophes. *Sci. Rep.* **2023**, *13*, 3649. [[CrossRef](#)] [[PubMed](#)]
6. Branca, S.; Del Carlo, P. Eruptions of Mt. Etna during the Past 3,200 Years: A Revised Compilation Integrating the Historical and Stratigraphic Records. In *Mt. Etna: Volcano Laboratory*; Geophysical Monograph Series; American Geophysical Union: Washington, DC, USA, 2004; Volume 143, pp. 1–27. ISBN 978-0-87590-408-5.
7. Gudmundsson, M.T.; Thordarson, T.; Höskuldsson, Á.; Larsen, G.; Björnsson, H.; Prata, F.J.; Oddsson, B.; Magnússon, E.; Högnadóttir, T.; Petersen, G.N.; et al. Ash Generation and Distribution from the April–May 2010 Eruption of Eyjafjallajökull, Iceland. *Sci. Rep.* **2012**, *2*, 572. [[CrossRef](#)]
8. Oxford Economics. *The Economic Impacts of Air Travel Restrictions Due to Volcanic Ash*; Oxford Economics: Oxford, UK, 2010; pp. 1–15.
9. Rodríguez-Hernández, Á.; Díaz-Díaz, R.; Zumbado, M.; Bernal-Suárez, M.d.M.; Acosta-Dacal, A.; Macías-Montes, A.; Travieso-Aja, M.d.M.; Rial-Berriel, C.; Henríquez Hernández, L.A.; Boada, L.D.; et al. Impact of Chemical Elements Released by the Volcanic Eruption of La Palma (Canary Islands, Spain) on Banana Agriculture and European Consumers. *Chemosphere* **2022**, *293*, 133508. [[CrossRef](#)]
10. Caricchi, L.; Townsend, M.; Rivalta, E.; Namiki, A. The Build-up and Triggers of Volcanic Eruptions. *Nat. Rev. Earth Environ.* **2021**, *2*, 458–476. [[CrossRef](#)]
11. Lewis, N.; Moretti, A. Understanding Volcano Hazards and Preventing Volcanic Disasters: A Science Strategy for the Volcano Hazards Program 2004–2008. In *Volcanoes: Formation, Eruptions and Modelling*; Nova Science Publishers: Hauppauge, NY, USA, 2009; pp. 243–314.
12. Sparks, R.S.J. Forecasting Volcanic Eruptions. *Earth Planet. Sci. Lett.* **2003**, *210*, 1–15. [[CrossRef](#)]
13. Sparks, R.S.J.; Biggs, J.; Neuberg, J.W. Monitoring Volcanoes. *Science* **2012**, *335*, 1310–1311. [[CrossRef](#)]
14. Tilling, R.I. The Critical Role of Volcano Monitoring in Risk Reduction. *Adv. Geosci.* **2008**, *14*, 3–11. [[CrossRef](#)]
15. Phillipson, G.; Sobradelo, R.; Gottsmann, J. Global Volcanic Unrest in the 21st Century: An Analysis of the First Decade. *J. Volcanol. Geotherm. Res.* **2013**, *264*, 183–196. [[CrossRef](#)]
16. Pallister, J.; McNutt, S.R. Chapter 66—Synthesis of Volcano Monitoring. In *The Encyclopedia of Volcanoes*, 2nd ed.; Sigurdsson, H., Ed.; Academic Press: Amsterdam, The Netherlands, 2015; pp. 1151–1171. ISBN 978-0-12-385938-9.
17. Reath, K.; Pritchard, M.; Poland, M.; Delgado, F.; Carn, S.; Coppola, D.; Andrews, B.; Ebmeier, S.K.; Rumpf, E.; Henderson, S.; et al. Thermal, Deformation, and Degassing Remote Sensing Time Series (CE 2000–2017) at the 47 Most Active Volcanoes in Latin America: Implications for Volcanic Systems. *J. Geophys. Res. Solid Earth* **2019**, *124*, 195–218. [[CrossRef](#)]
18. Corradini, S.; Guerrieri, L.; Stelitano, D.; Salerno, G.; Scollo, S.; Merucci, L.; Prestifilippo, M.; Musacchio, M.; Silvestri, M.; Lombardo, V.; et al. Near Real-Time Monitoring of the Christmas 2018 Etna Eruption Using SEVIRI and Products Validation. *Remote Sens.* **2020**, *12*, 1336. [[CrossRef](#)]
19. Guerrieri, L.; Merucci, L.; Corradini, S.; Pugnaghi, S. Evolution of the 2011 Mt. Etna Ash and SO<sub>2</sub> Lava Fountain Episodes Using SEVIRI Data and VPR Retrieval Approach. *J. Volcanol. Geotherm. Res.* **2015**, *291*, 63–71. [[CrossRef](#)]
20. Andronico, D.; Lodato, L. Effusive Activity at Mount Etna Volcano (Italy) During the 20th Century: A Contribution to Volcanic Hazard Assessment. *Nat. Hazards* **2005**, *36*, 407–443. [[CrossRef](#)]
21. Xu, W.; Xie, L.; Aoki, Y.; Rivalta, E.; Jónsson, S. Volcano-Wide Deformation after the 2017 Erta Ale Dike Intrusion, Ethiopia, Observed With Radar Interferometry. *J. Geophys. Res. Solid Earth* **2020**, *125*, e2020JB019562. [[CrossRef](#)]
22. Grainger, R.G.; Highwood, E.J. Changes in Stratospheric Composition, Chemistry, Radiation and Climate Caused by Volcanic Eruptions. *Geol. Soc. Lond. Spec. Publ.* **2003**, *213*, 329–347. [[CrossRef](#)]
23. Salgueiro, V.; Guerrero-Rascado, J.L.; Costa, M.J.; Román, R.; Cazorla, A.; Serrano, A.; Molero, F.; Sicard, M.; Córdoba-Jabonero, C.; Bortoli, D.; et al. Characterization of Tajogaite Volcanic Plumes Detected over the Iberian Peninsula from a Set of Satellite and Ground-Based Remote Sensing Instrumentation. *Remote Sens. Environ.* **2023**, *295*, 113684. [[CrossRef](#)]
24. Minnis, P.; Harrison, E.F.; Stowe, L.L.; Gibson, G.G.; Denn, F.M.; Doelling, D.R.; Smith, W.L. Radiative Climate Forcing by the Mount Pinatubo Eruption. *Science* **1993**, *259*, 1411–1415. [[CrossRef](#)]
25. Millán, L.; Santee, M.L.; Lambert, A.; Livesey, N.J.; Werner, F.; Schwartz, M.J.; Pumphrey, H.C.; Manney, G.L.; Wang, Y.; Su, H.; et al. The Hunga Tonga-Hunga Ha’apai Hydration of the Stratosphere. *Geophys. Res. Lett.* **2022**, *49*, e2022GL099381. [[CrossRef](#)]

26. Graf, H.-F.; Feichter, J.; Langmann, B. Volcanic Sulfur Emissions: Estimates of Source Strength and Its Contribution to the Global Sulfate Distribution. *J. Geophys. Res.* **1997**, *102*, 10727–10738. [[CrossRef](#)]
27. Takebayashi, M.; Onishi, M.; Iguchi, M. Large Volcanic Eruptions and Their Influence on Air Transport: The Case of Japan. *J. Air Transp. Manag.* **2021**, *97*, 102136. [[CrossRef](#)]
28. Krotkov, N.A.; Schoeberl, M.R.; Morris, G.A.; Carn, S.; Yang, K. Dispersion and Lifetime of the SO<sub>2</sub> Cloud from the August 2008 Kasatochi Eruption. *J. Geophys. Res.* **2010**, *115*, D00L20. [[CrossRef](#)]
29. Wang, J.; Park, S.; Zeng, J.; Ge, C.; Yang, K.; Carn, S.; Krotkov, N.; Omar, A.H. Modeling of 2008 Kasatochi Volcanic Sulfate Direct Radiative Forcing: Assimilation of OMI SO<sub>2</sub> Plume Height Data and Comparison with MODIS and CALIOP Observations. *Atmos. Chem. Phys.* **2013**, *13*, 1895–1912. [[CrossRef](#)]
30. van Thriel, C.; Schäper, M.; Kleinbeck, S.; Kiesswetter, E.; Blaszkewicz, M.; Golka, K.; Nies, E.; Raulf-Heimsoth, M.; Brüning, T. Sensory and Pulmonary Effects of Acute Exposure to Sulfur Dioxide (SO<sub>2</sub>). *Toxicol. Lett.* **2010**, *196*, 42–50. [[CrossRef](#)]
31. Hansell, A.; Oppenheimer, C. Health Hazards from Volcanic Gases: A Systematic Literature Review. *Arch. Environ. Health Int. J.* **2004**, *59*, 628–639. [[CrossRef](#)]
32. Manisalidis, I.; Stavropoulou, E.; Stavropoulos, A.; Bezirtzoglou, E. Environmental and Health Impacts of Air Pollution: A Review. *Front. Public Health* **2020**, *8*, 14. [[CrossRef](#)]
33. Pavlidou, E.; Hecker, C.; Van Der Werff, H.; Van Der Meijde, M. Study of Volcanic Activity at Different Time Scales Using Hypertemporal Land Surface Temperature Data: Study of Volcanic Activity With LST Data. *J. Geophys. Res. Solid Earth* **2017**, *122*, 7613–7625. [[CrossRef](#)]
34. Coppola, D.; Laiolo, M.; Cigolini, C.; Massimetti, F.; Delle Donne, D.; Ripepe, M.; Arias, H.; Barsotti, S.; Parra, C.B.; Centeno, R.G.; et al. Thermal Remote Sensing for Global Volcano Monitoring: Experiences From the MIROVA System. *Front. Earth Sci.* **2020**, *7*, 362. [[CrossRef](#)]
35. Ganci, G.; Harris, A.J.L.; Del Negro, C.; Guehenneux, Y.; Cappello, A.; Labazuy, P.; Calvari, S.; Gouhier, M. A Year of Lava Fountaining at Etna: Volumes from SEVIRI. *Geophys. Res. Lett.* **2012**, *39*, L06305. [[CrossRef](#)]
36. Gouhier, M.; Harris, A.; Calvari, S.; Labazuy, P.; Guéhenneux, Y.; Donnadieu, F.; Valade, S. Lava Discharge during Etna’s January 2011 Fire Fountain Tracked Using MSG-SEVIRI. *Bull. Volcanol.* **2012**, *74*, 787–793. [[CrossRef](#)]
37. Corradini, S.; Montopoli, M.; Guerrieri, L.; Ricci, M.; Scollo, S.; Merucci, L.; Marzano, F.S.; Pugnaghi, S.; Prestifilippo, M.; Ventress, L.J.; et al. A Multi-Sensor Approach for Volcanic Ash Cloud Retrieval and Eruption Characterization: The 23 November 2013 Etna Lava Fountain. *Remote Sens.* **2016**, *8*, 58. [[CrossRef](#)]
38. Wooster, M.J.; Roberts, G.; Freeborn, P.H.; Xu, W.; Govaerts, Y.; Beeby, R.; He, J.; Lattanzio, A.; Fisher, D.; Mullen, R. LSA SAF Meteosat FRP Products—Part 1: Algorithms, Product Contents, and Analysis. *Atmos. Chem. Phys.* **2015**, *15*, 13217–13239. [[CrossRef](#)]
39. Philpotts, A.R.; Ague, J.J. *Principles of Igneous and Metamorphic Petrology*, 3rd ed.; Cambridge University Press: Cambridge, UK, 2022; ISBN 978-1-108-63141-9.
40. Smith, A.M.S.; Wooster, M.J. Remote Classification of Head and Backfire Types from MODIS Fire Radiative Power and Smoke Plume Observations. *Int. J. Wildland Fire* **2005**, *14*, 249–254. [[CrossRef](#)]
41. Johnston, J.M.; Wooster, M.J.; Paugam, R.; Wang, X.; Lynham, T.J.; Johnston, L.M. Direct Estimation of Byram’s Fire Intensity from Infrared Remote Sensing Imagery. *Int. J. Wildland Fire* **2017**, *26*, 668–684. [[CrossRef](#)]
42. Barberi, F.; Carapezza, M.L.; Valenza, M.; Villari, L. The Control of Lava Flow during the 1991–1992 Eruption of Mt. Etna. *J. Volcanol. Geotherm. Res.* **1993**, *56*, 1–34. [[CrossRef](#)]
43. Harris, A.; Steffke, A.; Calvari, S.; Spampinato, L. Thirty Years of Satellite-Derived Lava Discharge Rates at Etna: Implications for Steady Volumetric Output. *J. Geophys. Res.* **2011**, *116*, B08204. [[CrossRef](#)]
44. Proietti, C.; Coltelli, M.; Marsella, M.; Martino, M.; Scifoni, S.; Giannone, F. Towards a Satellite-Based Approach to Measure Eruptive Volumes at Mt. Etna Using Pleiades Datasets. *Bull. Volcanol.* **2020**, *82*, 35. [[CrossRef](#)]
45. Bisson, M.; Spinetti, C.; Andronico, D.; Palaseanu-Lovejoy, M.; Fabrizia Buongiorno, M.; Alexandrov, O.; Cecere, T. Ten Years of Volcanic Activity at Mt Etna: High-Resolution Mapping and Accurate Quantification of the Morphological Changes by Pleiades and Lidar Data. *Int. J. Appl. Earth Obs. Geoinf.* **2021**, *102*, 102369. [[CrossRef](#)]
46. Longpré, M.-A. Reactivation of Cumbre Vieja Volcano. *Science* **2021**, *374*, 1197–1198. [[CrossRef](#)]
47. Branca, S.; Coltelli, M.; Groppelli, G.; Lentini, F. Geological Map of Etna Volcano, 1:50,000 Scale. *Ital. J. Geosci.* **2011**, *130*, 265–291. [[CrossRef](#)]
48. Stothers, R.B.; Rampino, M.R. Historic Volcanism, European Dry Fogs, and Greenland Acid Precipitation, 1500 B.C. to A.D. 1500. *Science* **1983**, *222*, 411–413. [[CrossRef](#)] [[PubMed](#)]
49. Calvari, S.; Nunnari, G. Etna Output Rate during the Last Decade (2011–2022): Insights for Hazard Assessment. *Remote Sens.* **2022**, *14*, 6183. [[CrossRef](#)]
50. Mulas, M.; Cioni, R.; Andronico, D.; Mundula, F. The Explosive Activity of the 1669 Monti Rossi Eruption at Mt. Etna (Italy). *J. Volcanol. Geotherm. Res.* **2016**, *328*, 115–133. [[CrossRef](#)]
51. Branca, S.; De Beni, E.; Proietti, C. The Large and Destructive 1669 AD Eruption at Etna Volcano: Reconstruction of the Lava Flow Field Evolution and Effusion Rate Trend. *Bull. Volcanol.* **2013**, *75*, 694. [[CrossRef](#)]
52. Archambault, C.; Tanguy, J.C. Comparative Temperature Measurements on Mount Etna Lavas: Problems and Techniques. *J. Volcanol. Geotherm. Res.* **1976**, *1*, 113–125. [[CrossRef](#)]

53. Klügel, A.; Hansteen, T.H.; Galipp, K. Magma Storage and Underplating beneath Cumbre Vieja Volcano, La Palma (Canary Islands). *Earth Planet. Sci. Lett.* **2005**, *236*, 211–226. [[CrossRef](#)]
54. Bonadonna, C.; Pistolesi, M.; Biass, S.; Voloschina, M.; Romero, J.; Coppola, D.; Folch, A.; D’Auria, L.; Martin-Lorenzo, A.; Dominguez, L.; et al. Physical Characterization of Long-Lasting Hybrid Eruptions: The 2021 Tajogaite Eruption of Cumbre Vieja (La Palma, Canary Islands). *J. Geophys. Res. Solid Earth* **2022**, *127*, e2022JB025302. [[CrossRef](#)]
55. Muñoz, V.; Walter, T.R.; Zorn, E.U.; Shevchenko, A.V.; González, P.J.; Reale, D.; Sansosti, E. Satellite Radar and Camera Time Series Reveal Transition from Aligned to Distributed Crater Arrangement during the 2021 Eruption of Cumbre Vieja, La Palma (Spain). *Remote Sens.* **2022**, *14*, 6168. [[CrossRef](#)]
56. Plank, S.; Shevchenko, A.V.; d’Angelo, P.; Gstaiger, V.; González, P.J.; Cesca, S.; Martinis, S.; Walter, T.R. Combining Thermal, Tri-Stereo Optical and Bi-Static InSAR Satellite Imagery for Lava Volume Estimates: The 2021 Cumbre Vieja Eruption, La Palma. *Sci. Rep.* **2023**, *13*, 2057. [[CrossRef](#)]
57. Durão, R.; Alonso, C.; Gouveia, C. The Performance of ECMWF Ensemble Prediction System for European Extreme Fires: Portugal/Monchique in 2018. *Atmosphere* **2022**, *13*, 1239. [[CrossRef](#)]
58. Pinto, M.M.; DaCamara, C.C.; Trigo, I.F.; Trigo, R.M.; Turkman, K.F. Fire Danger Rating over Mediterranean Europe Based on Fire Radiative Power Derived from Meteosat. *Nat. Hazards Earth Syst. Sci.* **2018**, *18*, 515–529. [[CrossRef](#)]
59. Durand, M.; Grattan, J. Effects of Volcanic Air Pollution on Health. *Lancet* **2001**, *357*, 164. [[CrossRef](#)]
60. CAMS Monitors Transport of SO<sub>2</sub> from La Palma Volcano | Copernicus. Available online: <https://atmosphere.copernicus.eu/cams-monitors-transport-so2-la-palma-volcano> (accessed on 11 September 2023).
61. Global Volcanism Program. Report on Etna (Italy). In *Bulletin of the Global Volcanism Network*; Smithsonian Institution: Washington, DC, USA, 2021; Volume 46. [[CrossRef](#)]
62. Global Volcanism Program | Report on Etna (Italy)—17 February–23 February 2021. Available online: <https://volcano.si.edu/ShowReport.cfm?vvar=GVP.WVAR20210217-211060> (accessed on 11 September 2023).
63. Global Volcanism Program | Report on Etna (Italy)—30 June–6 July 2021. Available online: <https://volcano.si.edu/ShowReport.cfm?vvar=GVP.WVAR20210630-211060> (accessed on 11 September 2023).
64. Global Volcanism Program. Report on La Palma (Spain). In *Bulletin of the Global Volcanism Network*; Smithsonian Institution: Washington, DC, USA, 2021; Volume 46. [[CrossRef](#)]
65. Wooster, M.J.; Roberts, G.; Perry, G.L.W.; Kaufman, Y.J. Retrieval of Biomass Combustion Rates and Totals from Fire Radiative Power Observations: FRP Derivation and Calibration Relationships between Biomass Consumption and Fire Radiative Energy Release. *J. Geophys. Res.* **2005**, *110*, D24311. [[CrossRef](#)]
66. Directive 2008/50/EC of the European Parliament and of the Council of 21 May 2008 on Ambient Air Quality and Cleaner Air for Europe; OJ L 152; Special edition in Croatian; European Parliament, Council of the European Union: London, UK, 2008; Volume 029.

**Disclaimer/Publisher’s Note:** The statements, opinions and data contained in all publications are solely those of the individual author(s) and contributor(s) and not of MDPI and/or the editor(s). MDPI and/or the editor(s) disclaim responsibility for any injury to people or property resulting from any ideas, methods, instructions or products referred to in the content.